CHAPTER «CHEMICAL SCIENCES»

PHASE EQUILIBRIA IN THE SYSTEMS WITH ZrO_2, CeO_2 AND Dy_2O_3

Oksana Kornienko[1]
Elena Andrievskaya[2]

DOI: https://doi.org/10.30525/978-9934-588-38-9-58

Abstract. The systems containing ceria, dysprosium and zirconia are perspective for the development of energy saving technological solutions and solid oxide fuel cells (SOFC). Ceramics based on ZrO_2 is used as a high temperature electrolyte for SOFC. The solid solutions based on CeO_2 are the most perspective electrolytes, operating at moderate temperatures, because of their ionic conductivity and high sensitivity to changes of oxygen partial pressure is much higher than ones of ZrO_2 stabilized with Y_2O_3 (YSZ).

In the present work, firstly, the phase equilibria and physicochemical properties for solid solutions in the ternary ZrO_2-CeO_2-Dy_2O_3 at temperatures 1100 and 1500°C (150 h) and binary CeO_2-Dy_2O_3 systems (1500 -600°C) in air were studied by X-ray diffraction and scanning electron microscopy in the overall concentration range of compositions.

Cerium oxide nitrate $Ce(NO_3)_3 \cdot 6H_2O$ and zirconium oxide nitrate $ZrO(NO_3)_2 \cdot 2H_2O$ of grade "ch" (above 98%, dysprosium oxide (99.99% produced by Merck Corp.) and analytical-grade nitric acid were used as the starting materials. Samples were prepared with a concentration step of 1-5 mol% from nitrate solutions with subsequent evaporation and decomposition of nitrates into oxides through annealing at 1200°C for 2 h. Powders were pressed in pellets (diameter 5 mm, height 4 mm) under a pressure of 10-30 MPa.

[1] PhD Physical Chemistry, Head of Unit «Functional ceramics based on rare earths»,
Institute for Problems of Materials Sciences of the Ukrainian Academy of Sciences, Ukraine
[2] Dr. Physical Chemistry,
Institute for Problems of Materials Sciences of the Ukrainian Academy of Sciences, Ukraine

Phase equilibriums and structure transformations in the CeO_2–Dy_2O_3 system have been studied within 1500 – 600°C in the full concentration range. It was established that the system is characterized by the formation of solid solutions on the basis of cubic modification of Dy_2O_3 (C-type) and fluorite CeO_2 (F-type). Solubility limits and concentration dependences of lattice parameters were determined for the phases forming in the system.

Any new phase in the ternary system was revealed at 1100 and 1500°C. The structure of the boundary binary systems defines the phase equilibria in the ZrO_2-CeO_2-Dy_2O_3 system. Solid solutions based on tetragonal (T) modification ZrO_2, cubic (C) modification Dy_2O_3 and cubic with fluorite-type structure (F) modifications CeO_2 (ZrO_2) were determined. The isothermal sections of the ZrO_2-CeO_2-Dy_2O_3 system at 1500°C contains two two-phase regions (F+C, T+F) and three two-phase regions (F+C, T+F, T+M) at 1100°C.

1. Introduction

Phase equilibria in the ZrO_2-CeO_2-Ln_2O_3 systems are important for the development of alternative ceramics for thermal barrier coatings (TBCs) other than state of the art yttria-stabilized zirconia (YSZ), aiming to lower thermal conductivity and to improve high temperature performance and durability. Ceria doped with aliovalent cations, such as rare earth oxides, has been considered as one of the most promising candidate materials for intermediate temperature solid oxide fuel cells (SOFCs) because of its much higher ionic conductivity at lower temperatures in comparison with that of stabilized zirconia. In addition, ceria finds its application in optical polishing, petroleum cracking catalyst, nuclear reactors components etc [1–6].

Albeit its great prospects for technological applications, the phase relationship of the ternary ZrO_2–CeO_2–Dy_2O_3 system has not been investigated in detail. The phase relations in the boundary of binary ZrO_2–CeO_2 and ZrO_2–Dy_2O_3, CeO_2–Dy_2O_3 systems have been studied [7–20].

The phase diagram of the ZrO_2–CeO_2 system is characterized by limited mutual solubility of their constituent oxides in the solid state. In the subsolidus area of the binary ZrO_2–CeO_2 phase diagram at 1500 and 1100°C, the following phases were revealed: monoclinic M -ZrO_2 in the range from 0 to 1 mol% CeO_2 (1100°C) and tetragonal T-ZrO_2 in the range from 0 to

18 mol% CeO_2 (1500°C) from 2 to 18 mol% CeO_2 (1100°C) and cubic, fluorite-type phase F-CeO_2 in the range from 56 to 100 mol% CeO_2 from 73 to 100 mol% CeO_2 (1100°C). The two-phase field (F+T) was established in the concentration range of 18–56 mol% CeO_2 at 1500°C and 18–73 mol% CeO_2 at 1100°C [7–10].

Phase equilibria in the CeO_2 based systems doped with REE oxides (La_2O_3, Sm_2O_3, Gd_2O_3, Er_2O_3, Dy or Yb_2O_3) have been partially studied [11–18]. It was established that equilibrium phases are substitutional solid solutions formed by four– and three-valence ions and containing high concentration of compensating defects such as oxygen vacancies and interstitial ions, which provide electric neutrality of the solution crystals. The information about phase equilibria in the CeO_2–Dy_2O_3 system is contradictory. Formation of solid solutions in the CeO_2–Dy_2O_3 system at 1400, 1500°C has been studied before [16–18]. The existence of solid solutions on the basis of F-CeO_2 and C-Dy_2O_3 at temperature 1400°C, was confirmed in [10], where the F – C transition was established in the concentration range 70% CeO_2. Herein no two-phase region was revealed [16; 17]. Furthermore, to our knowledge, there is no graphical representation of phase diagram for the CeO_2-Dy_2O_3 system in literature. The available information on phase relations in this system is contradictory, which demands additional studies. Therefore, the present work was aimed at constructing a low temperature part of binary phase diagram of the CeO_2-Dy_2O_3 system in the temperature range of 600-1500 °C using long-term annealing regimes at a partial oxygen pressure of 0.2 atm in air.

The phase relations in the boundary of binary ZrO_2–Dy_2O_3 system have been studied [19–27]. The phase diagram of the ZrO_2–Dy_2O_3 system is characterized by limited mutual solubility of their constituent oxides in the solid state. In the subsolidus area of the binary ZrO_2–CeO_2 phase diagram at 1500 and 1100°C, the following phases were revealed: tetragonal T-ZrO_2 in the range from 0 to 0.5 mol% Dy_2O_3 (1500–1100°C) and cubic, fluorite-type phase F-ZrO_2 in the range from 91 to 53 mol% ZrO_2 (1500°C) and from 88 to 66 mol% ZrO_2 (1100°C) and cubic modification of REE oxides C-Dy_2O_3 in the range from 69 to 100 mol% Dy_2O_3 (1500°C) and from 85 to 100 mol% Dy_2O_3 (1100°C). The two-phase field (F+T) was established in the concentration range of 0.5–9 mol% Dy_2O_3 at 1500°C and 0.5–12 mol% Dy_2O_3 at 1100°C [19; 20].

2. Experimental

Zirconium oxide nitrate, $ZrO(NO_3)_2 \cdot 2H_2O$, cerium oxide nitrate, $Ce(NO_3)_3 \cdot 6H_2O$, dysprosium oxide, Dy_2O_3 (all 99.99% produced by Merck Corp.) and analytical-grade nitric acid were used as the starting materials. The specimens were prepared in step 1-5 mol% Dy_2O_3 as follows: mixing the cerium and samarium nitrate solutions followed by their co-evaporation and calcination at 1000°C for 2 h until uniform mixtures of oxides formed. The as-prepared powders were pressed at 10 MPa into pellets of 5 mm in diameter and 4 mm in height. To study phase relationships at 1500°C, thermal treatment of as-prepared samples was carried out in two stages: at 1100°C (for 452 to 846h in air) and then at 1500°C (for 150 h in air) in the furnaces with heating elements based on Fecral (H23U5T) and Superkanthal ($MoSi_2$), respectively. The two-step annealing allows removing residuals of nitrogen oxides from the samples. At lower temperatures, ≤1250°C, phase equilibria (which include processes of disordering/ ordering) were reached rather slowly because of low velocity of diffusion processes in the cation sublattice, which requires long-term annealing of samples [28]. To study phase equilibria at 1100°C and 600°C, the heat treatment of the samples was carried out in air for 10813 to 16550 hours and 31500 hours, in respectively. The heating rate was 3.5°C min^{-1}. The cooling rate was about 100°C/min when switching off the power from the furnace. No phase composition changes were fixed at this rate or faster cooling. This technology of preparation does not influence the valence of rear earth elements.

XRD analysis of samples was performed by powder procedure on a DRON-3 apparatus at ambient temperature under CuKα radiation. Scanning step was 0.05-0.1° in the range 2θ=15–90°. Lattice parameters were calculated by the least square method using the LATTIC computer code with an error of not lower than 0.0001 nm for the cubic phase. The phase composition was determined using the "Match" program, which utilizes PDF-2 database of standard X-ray data. Diffraction peaks parameters determined by approximating the peaks of experimental diffractograms using the Voigt function, were used for the phase identification and calculations of lattice parameters.

Microstructures were examined on polished sections of annealed samples by electron-probe X-ray microanalysis (EPXMA) in backscattered electron, and secondary electron modes. Stoichiometric composition was controlled selectively by chemical and X-ray fluorescence spectrum analysis.

3. Results and Discussion

3.1. Interaction of ceria and dysprosia in air within temperature range 1500–600°C

The study of solid phase interaction of CeO_2 (fluorite type, F, space group $Fm\bar{3}m$) with Dy_2O_3 (cubic modification of REE oxides, C, space group $Ia\bar{3}$) in the temperature range of 600 – 1500°C revealed that in the CeO_2–Dy_2O_3 system two types of solid solutions are formed, which have a cubic structure: of fluorite F-CeO_2 (F-type) and C-Dy_2O_3 (C-type) separated by two-phase (F + C) region (Figure 1).

Table 1 contain data on the initial chemical and phase composition of samples annealed at 1500, 1100, and 600°C as well as on lattice parameters for phases that are in equilibrium at the corresponding temperatures.

Homogeneity region boundaries were determined for solid solutions on the basis of F-CeO_2 and C-Dyb_2O_3 as follows: contain 0–20 and 95–100 mol% Dy_2O_3 at 1500°C, 0–15 and 95–100 mol% Dy_2O_3 at1500°C, 0–10 and 95–100 mol.% Dy_2O_3 at 600°C, respectively (Table 1, Figure 1).

Dissolution of dysprosia in ceria during annealing in air proceeds by mutual diffusion and solid solution formation through different-valence substitution: Dy^{3+} ions substitute for Ce^{4+} ions in the F-type lattice sites. In order to preserve charge neutrality of the crystal, the difference in ion charge is compensated by the appearance of oxygen vacancies in sites of oxygen ions. Thus the F-CeO_2 lattice parameter reduces (Figure 2 and 3) owing to the difference in the cation sizes, on the one hand, and the sizes of oxygen ion and oxygen vacancy, on the other hand. There are however such solubility limit values which correspond to a critical concentration of vacancies, beyond of which the fluorite-type (*Fm3m)* lattice becomes unstable and transforms into another cubic lattice, namely *Ia3*, characteristic for solid solutions of the C-type on the basis of REE oxides. The solubility limit increases with temperature rising.

Lattice parameters F-CeO_2 decrease from a = 0.5409 nm for pure CeO_2 to a = 0.5394 nm (1500°C), 0.5396 nm (1100°C), and 0.5397 nm (600°C) for the limit solid solution compositions (Table 1, Figure 2). The XRD patterns that characterize solid solution regions in the CeO_2–Dy_2O_3 system at 1100°C are shown in Figure 3, where the presence of two phases is distinctly seen at any percentage of components and phases, which made it possible to carry out an accurate phase analysis.

The solubility of ceria in C– Dy_2O_3 is 9% at 1500°C and 4% at 600°C. The lattice parameter increases from a = 1.0655 nm for pure Dy_2O_3 to a = 1.0710 nm (1500°C) and to a = 1.0679 nm (1100°C) for the limit solid solution compositions and to a = 1.0678 nm for the sample containing 95 mol% Dy_2O_3 (1100°C).

Formation of substitutional solid solutions is accompanied with charge compensation, since ion Dy^{3+} is replaced by ion Ce^{4+}. The excess positive charge is neutralized *via* placing of oxygen ions in intersites or catching electrons. An increase in the concentration of ceria (with larger cerium ion) in the solid solution results in increasing lattice parameter. The solubility limit is responsible for formation of F-type solid solutions.

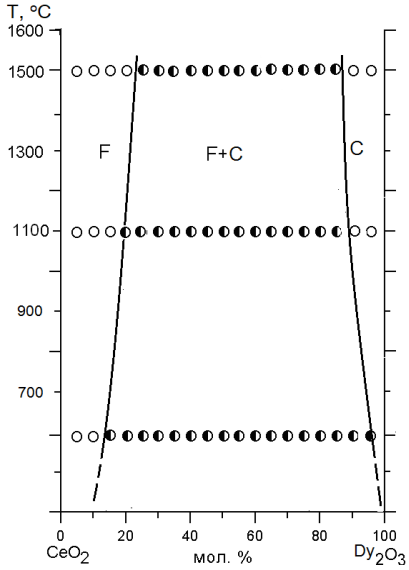

Figure 1. Phase equilibriums in the CeO_2-Dy_2O_3 system within 600-1500°C: ○, single-phase samples; ◑, two-phase samples.

3.2. Phase relation studies in the ZrO_2-CeO_2– Dy_2O_3 system at 1500 and 1100°C

To study the phase equilibria in the ZrO_2–CeO_2–Dy_2O_3 system, the following experimental parameters were selected to elucidate the location of the

Table 1

Phase composition and lattice parameters of the phases in the CeO_2–Dy_2O_3 system, annealed at 1500°C for 150 h, 1100°C for 16550 h, 600°C for 31500 h (XRD data)

Chemical composition mol%		Phase composition T=1500°C	Lattice parameters of the phases (nm) ($a \pm 0.0002$) T = 1500°C		Phase composition T=1100°C	Lattice parameters of the phases (nm) ($a \pm 0.0002$) T = 1100°C		Phase composition T=600°C	Lattice parameters of the phases (nm) ($a \pm 0.0002$) T = 600°C	
CeO_2	Dy_2O_3		<F>	<C>		<F>	<C>		<F>	<C>
0	100	<C>	—	1.0655	<C>	-	1.0655	<C>	-	1.0655
5	95	<C>	—	1.0675	<C>	-	1.0679	<C>+ <F>	-	1.0678
10	90	<C>	—	1.0710	<C> +<F>	-	1.0709	<C> + <F>	-	1.0673
15	85	<C> + <F>	—	1.0740	<C> +<F>	0.5394	1.0707	<C> + <F>	-	1.0675
20	80	<C> + <F>	0.5392	1.0735	<C> + <F>	0.5394	1.0709	<C> + <F>	0.5400	1.0677
25	75	<C> + <F>	0.5394	1.0735	<C> + <F>	0.539	1.0699	<C> + <F>	0.5399	1.0677
30	70	<C> + <F>	0.5391	1.074	<C> + <F>	0.5393	1.0709	<C> + <F>	0.5401	1.0679
35	65	<C> + <F>	0.5393	1.073	<C> + <F>	0.5395	1.071	<C> + <F>	0.5399	1.067
40	60	<C> + <F>	0.5393	1.0744	<C> + <F>	0.5394	1.0709	<C> + <F>	0.5400	1.0679
45	55	<C> + <F>	0.5392	1.0739	<C> + <F>	0.5393	1.0712	<C> + <F>	0.5399	1.0677
50	50	<C> + <F>	0.5392	1.0741	<C> + <F>	0.5394	1.0703	<C> + <F>	0.5398	1.0677
55	45	<C> + <F>	0.5393	1.0738	<C> + <F>	0.5395	1.0708	<C> + <F>	0.5398	1.0675
60	40	<C> + <F>	0.5393	1.074	<C> + <F>	0.5394	1.0706	<C> + <F>	0.5400	1.0679
65	35	<C> + <F>	0.5393	1.0735	<C> + <F>	0.5394	1.0701	<C> + <F>	0.5399	1.0679
70	30	<C> + <F>	0.5392	1.074	<C> + <F>	0.5393	1.0708	<C> + <F>	0.5398	1.0679
75	25	<C> + <F>	0.5393	—	<C>+<F>	0.5392	-	<C> + <F>	0.5399	1.0676
80	20	<F>	0.5394	—	<C>+<F>	0.5394	-	<F>	0.5497	-
85	15	<F>	0.5397	—	<F>	0.5396	-	<F>	0.5399	-
90	10	<F>	0.5402	—	<F>	0.5402	-	<F>	0.5403	-
95	5	<F>	0.5405	—	<F>	0.5405	-	<F>	0.5405	-
100	0	<F>	0.5409	—	<F>	0.5409	-	<F>	0.5409	-

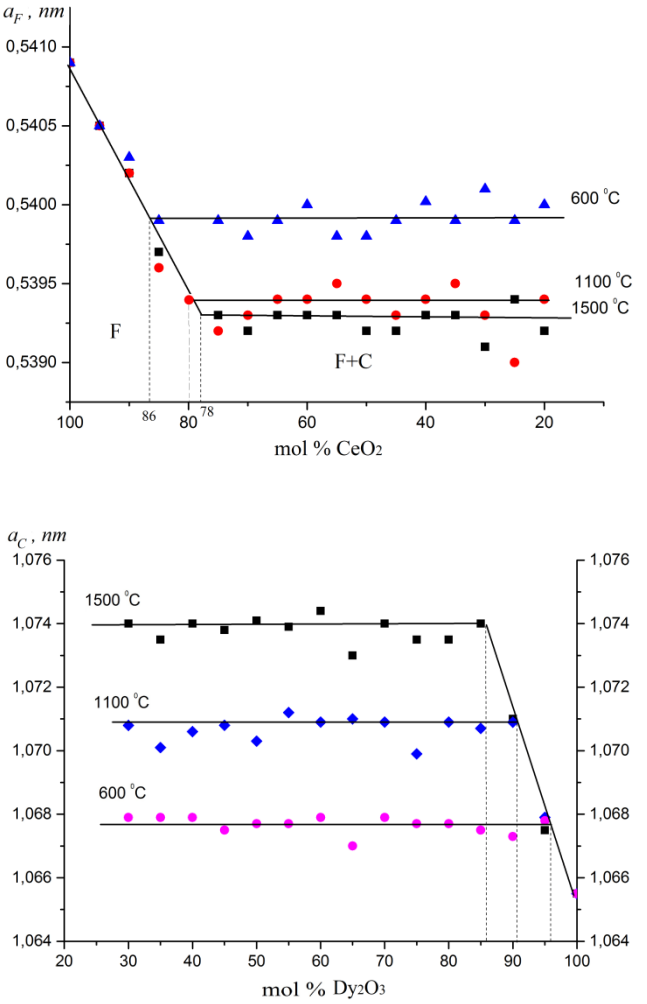

Figure 2. Concentration dependence of lattice parameters for solid solutions on the basis of *a* – F-CeO_2 and *b* – C-Dy_2O_3 in the CeO_2 – Dy_2O_3 system after annealing of samples at 1500, 1100 and 600°C

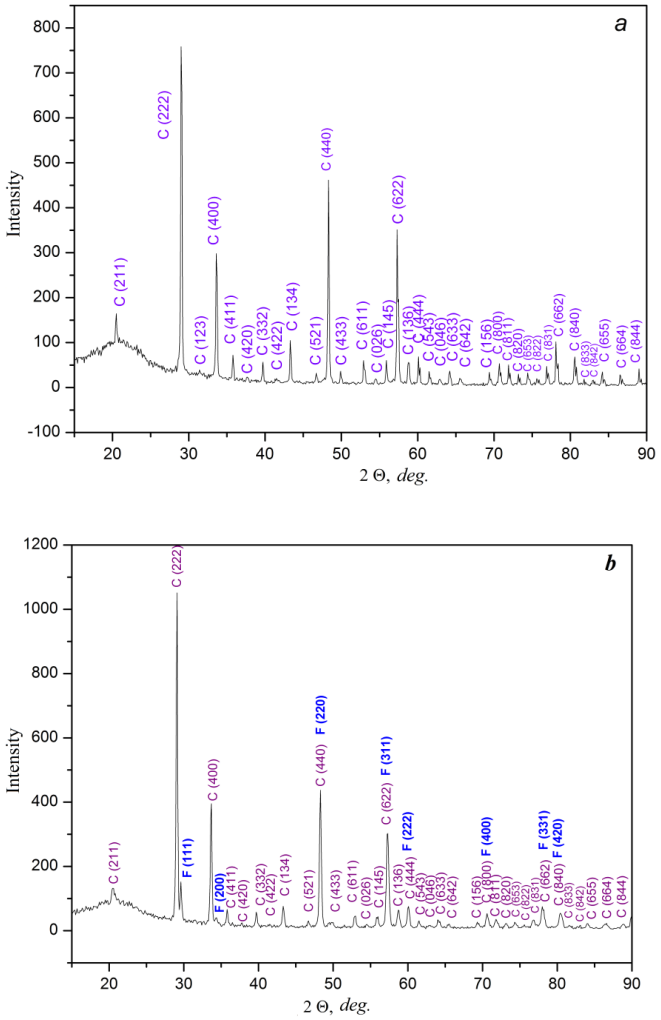

Figure 3. XRD patterns from $CeO_2 – Dy_2O_3$ samples annealed at 1100°C: *a* – 100 mol % Dy_2O_3, (C); *b* - 15 mol % CeO_2 – 85 mol % Dy_2O_3, (C + F)

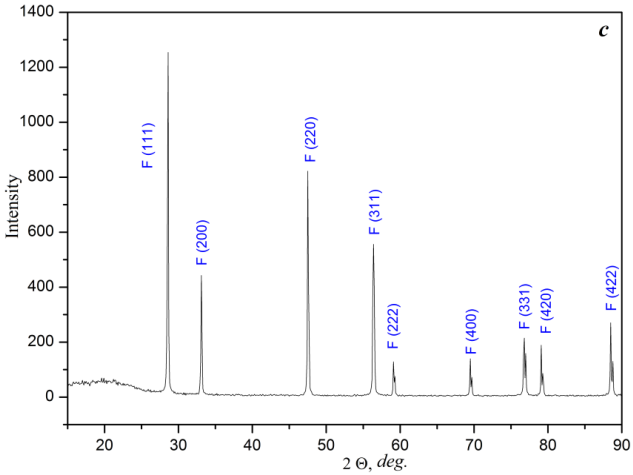

Figure 3. XRD patterns from CeO_2 – Dy_2O_3 samples annealed at 1100°C: *c* – 90 mol % CeO_2 –10 mol % Dy_2O_3, (F)

two lines: ZrO_2–(50 mol.% CeO_2–50 mol.% Dy_2O_3), CeO_2–(45 mol.% ZrO_2 – 55 mol.% Dy_2O_3) and two additional isoconcentrations of 20 mol% ZrO_2 and 70 mol% Dy_2O_3 compositions were included to clarify the phase diagram.

Figures 4 and 5 depicts the summary of experimental data for the isothermal section of the ZrO_2–CeO_2–Dy_2O_3 system at 1100 and 1500°C. The samples were annealed at 1100 and 1500°C in air and characterized by X-ray analysis and scanning electron microscope. Tables 2 and 3 summarize starting compositions, lattice parameters and compare the phase identification determined by X-ray.

Figures 6-8 demonstrate concentration dependences of solid solutions based on F-CeO_2 in the ZrO_2–CeO_2–Dy_2O_3 system after annealing at 1500 1100°C. XRD patterns acquired from in the ZrO_2–CeO_2–Dy_2O_3 system at 1100°C are presented in Figure 9.

In the zirconia-rich corner, the solid solutions based on tetragonal modification of ZrO_2 are formed. The phase field T-ZrO_2 is narrow and elongated (0–18 mol% at 1500°C and 0–18 mol% at 1100° CeO_2) along the ZrO_2–CeO_2 side of the binary system. The solubility of Dy_2O_3 in the T-ZrO_2 is low and amounts to ~ 0.5 mol% (at 1500 and 1100°C), as evidenced by XRD

analysis results. The boundary of the T phase in equilibrium with F-CeO_2 at 1500°C was determined from the XRD data for the: 99 mol.% ZrO_2–0,5 mol. % CeO_2–0,5 mol.% Dy_2O_3, 98 mol.% ZrO_2–1 mol. % CeO_2–1 mol.% Dy_2O_3, 97 mol.% ZrO_2–1,5 mol. % CeO_2–1,5 mol.% Dy_2O_3, 96 mol.% ZrO_2–2 mol. % CeO_2–2 mol.% Dy_2O_3, 95 mol.% ZrO_2–2,5 mol. % CeO_2–2,5 mol.% Dy_2O_3, 90 mol.% ZrO_2–5 mol. % CeO_2–5 mol.% Dy_2O_3, 85 mol.% ZrO_2–7,5 mol. % CeO_2–7,5 mol.% Dy_2O_3.

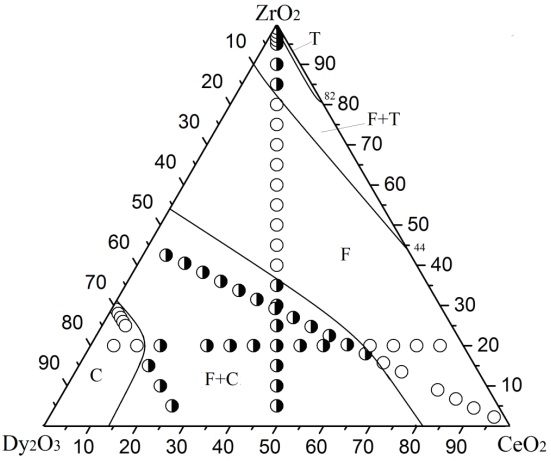

Figure 4. Isothermal section at 1500°C for the system ZrO_2–CeO_2–Dy_2O_3 (○ – single-phase samples; ◐ – two-phase samples.)

The boundary of the T phase in equilibrium with F-CeO_2 at 1100°C was determined from the XRD data for the: 99 mol.% ZrO_2–0,5 mol. % CeO_2–0,5 mol.% Dy_2O_3, 98 mol.% ZrO_2–1 mol. % CeO_2–1 mol.% Dy_2O_3, 97 mol.% ZrO_2–1,5 mol. % CeO_2–1,5 mol.% Dy_2O_3, 96 mol.% ZrO_2–2 mol. % CeO_2–2 mol.% Dy_2O_3, 95 mol.% ZrO_2–2,5 mol. % CeO_2–2,5 mol.% Dy_2O_3, 90 mol.% ZrO_2–5 mol. % CeO_2–5 mol.% Dy_2O_3, 85 mol.% ZrO_2–7,5 mol. % CeO_2–7,5 mol.% Dy_2O_3, 80 mol.% ZrO_2–10 mol. % CeO_2–10 mol.% Dy_2O_3. It is worth noting that the solid solutions based on tetragonal modification of zirconia cannot be quenched from high temperatures due to low stability of T-ZrO_2 under cooling with furnace conditions. The diffraction patterns recorded at room temperatures included the peaks of monoclinic phase

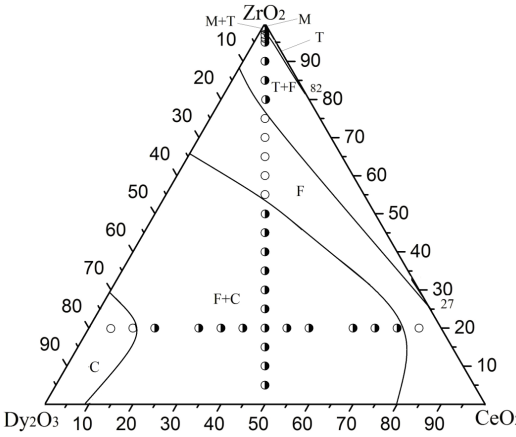

Figure 5. Isothermal section at 1500°C for the system ZrO_2–CeO_2–Dy_2O_3 (○ – single-phase samples; ◐ – two-phase samples.)

M-ZrO_2, but for the series of compositions, the partial stabilization of the tetragonal phase was found (Tables 2, 3).

The excess concentration of compensating vacancies in the oxygen sublattice and presence of ions larger than zirconium ions, both promote transformation of martensitic type in ZrO_2 at temperatures lower than 1170°C in pure oxide. At high ZrO_2 contents, the system contains M-ZrO_2 – based solid solutions (1100°C). Their phase field, narrow and elongated (0–99,5 mol% ZrO_2), extends along the ZrO_2–CeO_2 and ZrO_2–Dy_2O_3 side of the composition triangle. CeO_2 solubility in M-ZrO_2 does not exceed 0.5 mol%.

The microstructures (1500°C) shown in Figures 10 b-g are typical of T + F two-phase samples. The 85 mol% ZrO_2-7.5 mol% CeO_2-7.5 mol% Dy_2O_3, 90 mol% ZrO_2-5 mol% CeO_2-5 mol% Dy_2O_3, 90 mol% ZrO_2-8.5 mol% CeO_2–1.5 mol% Dy_2O_3, 95 mol% ZrO_2-2.5 mol% CeO_2-2.5 mol% Dy_2O_3 samples consist of two microstructural constituents differing notably in contrast. X-ray line scans show that the light phase, forming a matrix in the form of polyhedral grains 5 to 15 μm in size, is cerium-rich, suggesting that it is F-CeO_2. The gray phase contains zirconium, is present in a notably biggest amount, and consists of darker grains. These data suggest that this phase is T-ZrO_2, in accordance with XRD data. The 99 mol% ZrO_2 – 0.5 mol% CeO_2 – 0.5 mol% Dy_2O_3 sample contains a larger amount of the T phase, consisting

Table 2

Phase composition and lattice parameters of the phases in the ZrO_2–CeO_2–Dy_2O_3 system, annealed at 1500°C for 150 h (XRD data)

Chemical composition (mol%)			Phase composition and lattice parameters of the phases (nm)	Lattice parameters of the phases (nm) (a ±	
ZrO_2	CeO_2	Dy_2O_3		<F>	<C >
1	2	3	4	5	6
Section ZrO_2 - (50 ml. % CeO_2 - 50 mol. % Dy_2O_3)					
5	47.5	47.5	<F>+<C>	0.5367	-
10	45	45	<F>+<C>	0.5350	-
15	42.5	42.5	<F>+<C>	0.5350	-
20	40	40	<F>+<C>	0.5335	-
25	37.5	37.5	<F>+<C>	0.5424	-
30	35	35	<F>+<C>	0.5316	-
35	32.5	32.5	<F>+<C>	0.5305	
40	30	30	<F>	0.5293	-
45	27.5	27.5	<F>	0.5283	-
50	25	25	<F>	0.5266	-
55	22.5	22.5	<F>	0.5249	-
60	20	20	<F>	0.5244	-
65	17.5	17.5	<F>	0.5215	
70	15	15	<F>	0.5202	-
75	12.5	12.5	<F>	0.5187	-
80	10	10	<F>	0.5172	-
85	7.5	7.5	<F> оСн.+ <T>хх (a = 0.521, b = 0.5392, c = 0.5223, b	0.5158	-

End of Table 1

1	2	3	4	5	6
90	5	5	<F> + <T>xx↑ (a = 0.532, b = 0.5331, c = 0.5309, b	0.5152	-
95	2.5	2.5	<F> + <T>xx↑ (a = 0.526, b = 0.5211, c = 0.5410, b	0.5141	-
96	2	2	<F>↓ + <T>xx↑ (a = 0.521, b = 0.5196, c = 0.5416, b	0.5147	-
97	1.5	1.5	<F>↓ + <T>xx↑ (a = 0.521, b = 0.5194, c = 0.5557, b	-	
98	1	1	<F>↓+ <T>xx↑ (a = 0,521; b = 0,5199; c = 0,5470; b	-	-
99	0.5	0.5	<F>Сл. + <T>xx (a = 0,527; b = 0,5259; c = 0,5275; b		
Section CeO_2 - (45 mol. % ZrO_2 - 55 mol. % Dy_2O_3)					
42.5	5	52.5	<F>+<C>	0.5271	-
40.5	10	49.5	<F>+<C>	0.5278	-
38.25	15	46.75	<F>+<C>	0.5288	-
36	20	44	<F>+<C>	0.5299	-
33.75	25	41.25	<F>+<C>	0.5303	-
31.5	30	38.5	<F>+<C>	0.5308	-
29.25	35	35.75	<F>+<C>	0.5316	-
27	40	33	<F>+<C>	0.5324	-
24.75	45	30.25	<F>+<C>	0.5333	-

*At given conditions (T=1500°C for 150 h in air) the tetragonal modification of T-ZrO_2 does not become hardened, instead of it was observed the formation of monoclinic modification of M-ZrO_2. Designation of phases: <T> solid solutions based on tetragonal modification of ZrO_2, <C> solid solutions based on cubic modification of Dy_2O_3; <F> solid solutions based on cubic modification with fluorite-type structure of $ZrO_2(CeO_2)$

Table 3

Phase composition and lattice parameters of the phases in the ZrO_2–CeO_2–Dy_2O_3 system, annealed at 1100°C for 12475 h (XRD data)

Chemical composition (mol%)			Phase composition and lattice parameters of the phases (nm)	lattice parameters of the phases (nm) ($a \pm 0.0002$)	
ZrO_2	CeO_2	Dy_2O_3		<F>	<C >
1	2	3	4	5	6
Section ZrO_2 - (50 mol. % CeO_2 - 50 mol. % Dy_2O_3)					
5	47.5	47.5	<F>+<C>	0.5372	1.0737
10	45	45	<F>+<C>	0.5365	1.0732
15	42.5	42.5	<F>+<C>	0.5374	1.0739
20	40	40	<F>+<C>	0.5342	1.0683
25	37.5	37.5	<F>+<C>	0.5335	1.0671
30	35	35	<F>+<C>	0.5342	1.0684
35	32.5	32.5	<F>+<C>	0.5310	1.0641
40	30	30	<F>+<C>	0.5283	1.0656
45	27.5	27.5	<F>+<C>	0.5260	-
50	25	25	<F>	0.5261	-
55	22.5	22.5	<F>	0.5241	-
60	20	20	<F>	0.5225	-
65	17.5	17.5	<F>	0.5216	
70	15	15	<F>	0.5196	-
75	12.5	12.5	<F>	0.5189	-
80	10	10	<F>	0.5170	-
85	7.5	7.5	<F> оСн.+ <T>хх	0.5174	-

End of Table 2

1	2	3	4	5	6
90	5	5	<F> + <T>xx↑ (a = 0.606, b = 0.3999, c = 0.5437, β	0.5177	-
96	2	2	<F> + <T>xx↑ (a = 0.525, b = 0.5215, c = 0.5358, β	0.5154	-
97	1.5	1.5	<F>↓ + <T>xx↑ (a = 0.525, b = 0.5218, c = 0.5216, β	-	
98	1	1	<F>↓+ <T>xx↑ (a = 0.518, b = 0.5194, c = 0.5267, β	-	-
99	0.5	0.5	<F>Сл. + <T>xx (a = 0.517, b = 0.5188, c = 0.5260, β	-	-
Isoconcentrate 20 mol. % ZrO_2					
20	5	75	<C>	-	1.062
20	10	70	<C>	0.5311	1.063
20	15	65	<F>+<C>	0.5320	1.063
20	25	55	<F>+<C>	0.5317	1.063
20	30	50	<F>+<C>	0.5337	1.066
20	35	45	<F>+<C>	0.5281	1.056
20	45	35	<F>+<C>	0.5344	1.068
20	50	30	<F>+<C>	0.5361	1.072
20	60	20	<F>+<C>	0.5372	1.057
20	65	15	<F>+<C>	0.5383	1.0765
20	70	10	<F>+<C>	0.5394	1.0789
20	75	5	<F>	0.5360	-

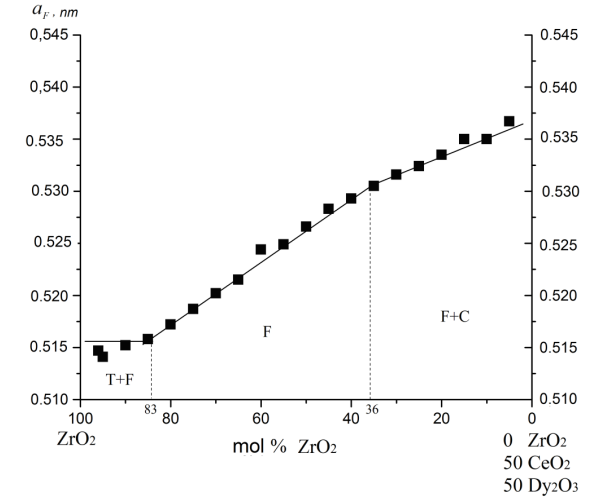

Figure 6. Concentration dependences of lattice parameters for solid solutions based on fluorite-type (F) along the ZrO_2– (50 мол. % CeO_2–50 мол. % Dy_2O_3) section in the system ZrO_2–CeO_2–Dy_2O_3 heat treated at 1500°C

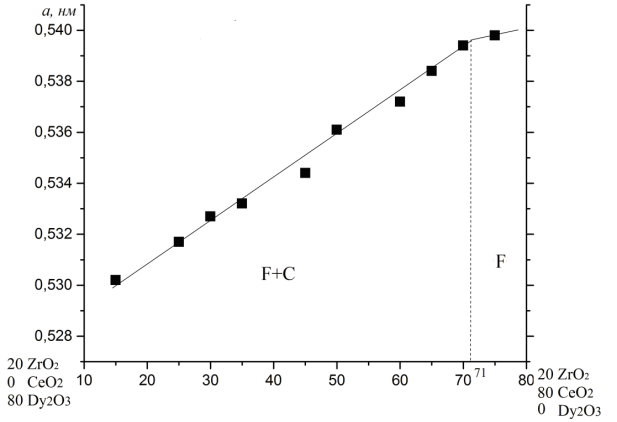

Figure 7. Concentration dependences of lattice parameters for solid solutions based on fluorite-type (F) along the Isoconcentrate 20 mol. % ZrO_2 in the system ZrO_2–CeO_2–Dy_2O_3 heat treated at 1100°C

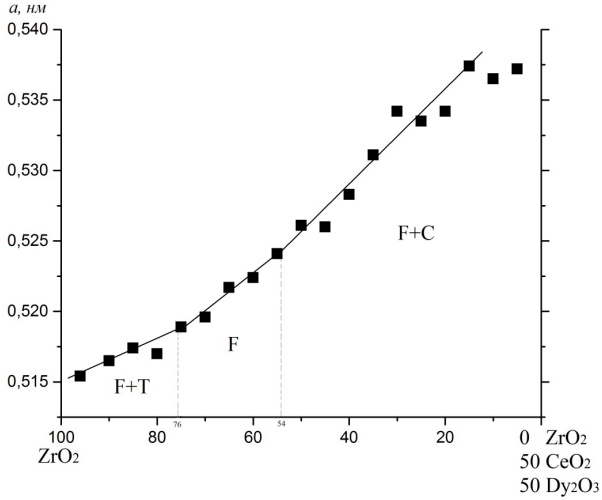

Figure 8. Concentration dependences of lattice parameters for solid solutions based on fluorite-type (F) along the ZrO_2– (50 мол. % CeO_2–50 мол. % Dy_2O_3) section in the system ZrO_2–CeO_2–Dy_2O_3 heat treated at 1100°C

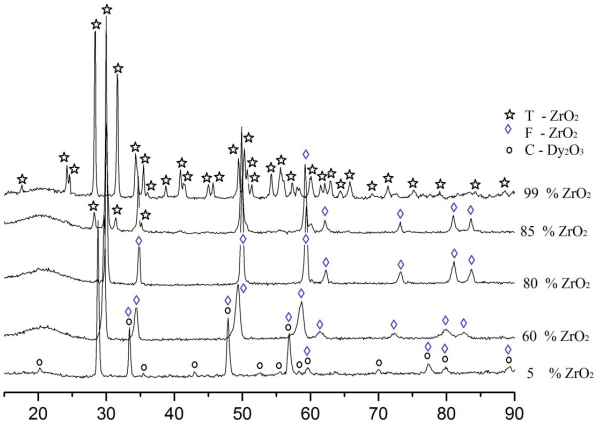

Figure 9. XRD patterns along the isoconcentrate 20 mol. % ZrO_2 in the system ZrO_2–CeO_2–Dy_2O_3 heat treated at 1100°C

of coarser grains. It differs in morphology from that in the above sample in that it has sharper grain boundaries (Figure 10 g). In the dysprosium-rich corner, the solid solutions based on cubic modification of Dy_2O_3 are formed. These solid solutions have cubic structure, the derivative from fluorite-type structure. As a result of replacing ions in the $CeO_2(ZrO_2)$ lattice by Dy^{3+}, oxygen vacancies arise, excess concentration of which acts as a driving force for ordering C-type phases. The model of substitution-type solid solution based on MeO_2 (Me = Ce, Zr) can be presented by Kröger-Vink formula: $Me_{1-x}Ln_xO_{2-x/2}$. The homogeneity field of C-phase was revealed to extend from 0 to 11 mol% CeO_2 along the isoconcentrate 20 mol% Dy_2O_3 at 1500 and 1100°C. The lattice parameter increases from a = 1.0585 nm for the sample containing 29 mol% ZrO_2-1 mol% CeO_2 – 70 mol% Dy_2O_3 to a = 1.0642 nm for the two-phase (F+C) sample containing 15 mol% ZrO_2-15 mol% CeO_2 – 70 mol% Dy_2O_3 along the isoconcentrate 70 mol% Dy_2O_3 at 1500°C. The lattice parameter increases from a = 1.0620 nm for the sample containing 20 mol% ZrO_2-5 mol% CeO_2 – 75 mol% Dy_2O_3 to a = 1.0630 nm for the two-phase (F+C) sample containing 20 mol% ZrO_2-15 mol% CeO_2 – 65 mol% Dy_2O_3 along the isoconcentrate 20 mol% Dy_2O_3 at 1100°C. The lattice parameter of the C-type solid solution increases with increasing Ce^{4+} content, but not only because of the steric factor. This may be associated with competition between these factors in the case of aliovalent substitution. When Ce^{4+} diffuses into the Dy_2O_3 lattice, there excess of anions, namely interstitial oxygen ions O^{2-}, appears for compensation of the excess positive charge. With increasing number of Ce^{4+} ions, the average cation radius slightly change but repulsion between the excess anions becomes stronger and provokes a dilatation effect in the lattice.

The microstructures, characterizing the two-phase field (C+F) are presented in Figures 10 h-j. In the samples containing 15 mol% ZrO_2 – 42.5 mol% CeO_2 – 42.5 mol% Dy_2O_3 and 20 mol% ZrO_2-15 mol% CeO_2 – 65 mol% Dy_2O_3, there are two structure components that differ by contrast. From the data of electron microprobe and X-ray spectral analysis, the light phase contains only dysprosium, and therefore, is a solid solution of C– Dy_2O_3. The dark phase is rich in cerium corresponding to the cubic solid solution F-CeO_2.

The cubic solid solution has a fluorite-type structure and homogeneity field shows the maximum extension. The boundary of the homogeneity field of F-phase passes through appropriate points in the binary ZrO_2–

CeO_2 (56 mol% CeO_2) and CeO_2–Dy_2O_3 (78 mol% CeO_2) and ZrO_2–Dy_2O_3 (91 – 53 mol% ZrO_2) systems at 1500°C (Figure 7). With decreasing temperature from 1500°C down to 1100°C, the homogeneity region on the basis of the cubic modification F-CeO_2 narrows. The boundary of the homogeneity field of F-phase passes through appropriate points in the binary ZrO_2–CeO_2 (73 mol% CeO_2) and CeO_2–Dy_2O_3 (80 mol% CeO_2) and ZrO_2–Dy_2O_3 (88 – 66 mol% ZrO_2) systems at 1100°C (Figure 8).

The lattice parameter decreases from a = 0.5367 nm for the two-phase (F+C) sample containing 5 mol% ZrO_2-47.5 mol% CeO_2 – 47.5 mol% Dy_2O_3 to a = 0.5293 nm for sample containing 40 mol% ZrO_2-30 mol% CeO_2 – 30 mol% Dy_2O_3 and to a = 0.5158 nm for sample containing 85 mol% ZrO_2-7.5 mol% CeO_2 – 7.5 mol% Dy_2O_3 along the Section ZrO_2 – (50 ml.% CeO_2 – 50 mol.% Dy_2O_3), (fig. 6, 1500°C). The lattice parameter increases from a = 0.5271 nm for the two-phase (F+C) sample containing 42.5 mol% ZrO_2 – 5 mol% CeO_2 – 52.5 mol% Dy_2O_3 to a = 0.5356 nm for sample containing 15.75 mol% ZrO_2-65 mol% CeO_2 – 19.25 mol% Dy_2O_3 along the Section CeO_2 – (45 mol.% ZrO_2 – 55 mol.% Dy_2O_3) at 1500°C.

The lattice parameter increases from a = 0.5320 nm for the two-phase (F+C) sample containing 20 mol% ZrO_2 – 15 mol% CeO_2 – 65 mol% Dy_2O_3 to a = 0.5360 nm for sample containing 20 mol% ZrO_2-75 mol% CeO_2 – 5 mol% Dy_2O_3 along the isoconcentrate 20 mol% ZrO_2 at 1100°C (fig. 7). The lattice parameter decreases from a = 0.5372 nm for the two-phase (F+C) sample containing 5 mol% ZrO_2 – 47.5 mol% CeO_2 – 47.5 mol% Dy_2O_3 to a = 0.5261 nm for sample containing 50 mol% ZrO_2-25 mol% CeO_2 – 25 mol% Dy_2O_3 and to a = 0.5174 nm for sample containing 85 mol% ZrO_2 – 7.5 mol% CeO_2 – 7.5 mol% Dy_2O_3 along the Section ZrO_2 – (50 ml.% CeO_2 – 50 mol.% Dy_2O_3), (fig. 8, 1100°C). The microstructures shown in Fig. 10 a, k, l are typical of phase-pure F-CeO_2(ZrO_2). The fluorite phase is also present in the two-phase (T + F and C + F).

4. Conclusions

Firstly, the phase equilibria in the systems ZrO_2–CeO_2–Dy_2O_3 and CeO_2–Dy_2O_3 has been studied in the whole concentration range. Phase equilibriums in the binary CeO_2-Dy_2O_3 system have been studied in the temperature range 600 – 1500 °C in air. It was established that the system is characterized by formation of limit solid solutions with a cubic structure

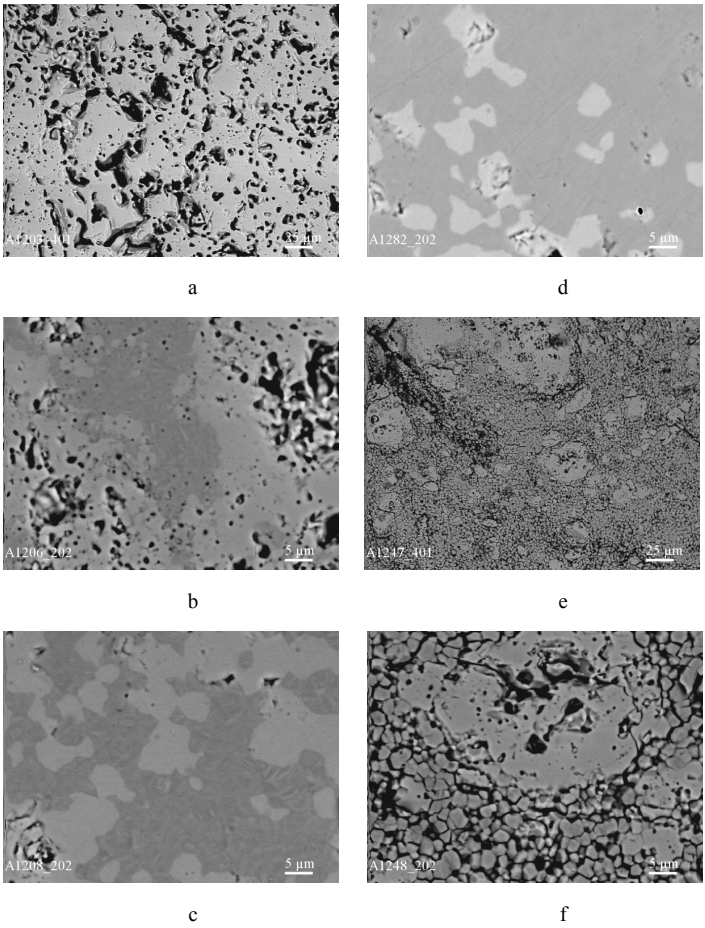

Figure 10. Microstructure of the ZrO_2–CeO_2–Dy_2O_3 system samples upon annealing at 1500°C according to BEI findings:
(a) 80%ZrO_2 – 10% CeO_2-10% Dy_2O_3, BEI×400, (F); **(b)** 85% ZrO_2– 7.5% CeO_2 – 7.5% Dy_2O_3, BEI×2000, (F+T) ; **(c)** 90% ZrO_2– 5% CeO_2 – 5% Dy_2O_3, BEI×2000, (F+T); **(d)** 90% ZrO_2 – 8.5% CeO_2 – 1.5% Dy_2O_3, BEI×2000, (F+T); **(e)** 95% ZrO_2 – 2.5% CeO_2 – 2.5% Dy_2O_3, BEI×2000 (F+T); **(f)** 95% ZrO_2 – 2.5% CeO_2 – 2.5% Dy_2O_3, BEI×400 (F+T); Light grains – (F-ZrO_2); Gray grains (T-ZrO_2); Black-pores

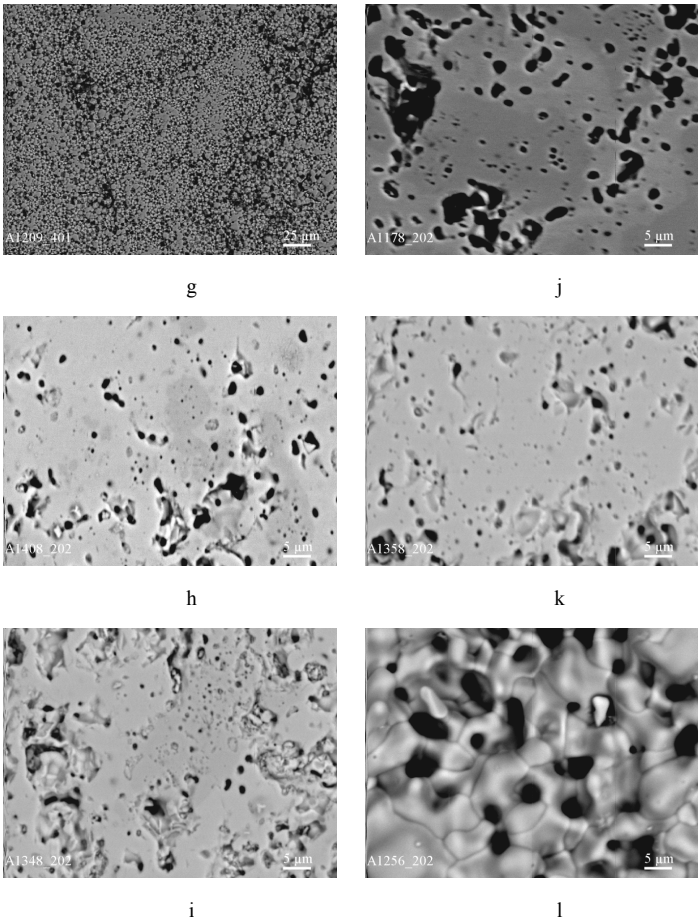

Figure 10 (page 2). Microstructure of the ZrO_2–CeO_2–Dy_2O_3 system samples upon annealing at 1500°C according to BEI findings:
(g) 99% ZrO_2 – 0.5% CeO_2 – 0.5% Dy_2O_3, BEI×400 (F+T); **(h)** 20% ZrO_2 – 15% CeO_2 – 65% Dy_2O_3, BEI×2000, (F+C) **(i)** 20% ZrO_2 – 10% CeO_2 – 70% Dy_2O_3, BEI×2000; (C) **(j)** 15% ZrO_2 – 42.5% CeO_2 – 42.5% Dy_2O_3, BEI×2000; (F+C) **(k)** 20% ZrO_2 – 60% CeO_2 – 20% Dy_2O_3, BEI×2000 (F), **(l)** 20% ZrO_2 – 68% CeO_2 – 12% Dy_2O_3, BEI×2000. **(F).** Light grains – (F-ZrO_2); Gray grains (T-ZrO_2); Black-pores

of two types, F-CeO_2 and C-Dy_2O_3, which are separated by a two-phase region, (C + F); formation of new phases does not occur even at the maximal annealing time. As temperature reduces from 1500 to 600°C, the homogeneity regions of solid solutions based on the cubic modifications F-CeO_2 and C-Dy_2O_3 narrow from 78 to 86% CeO_2 and from 14 to 4% CeO_2, respectively. In this temperature range, ordering of intermediate phases was not confirmed.

The isothermal section in the ternary system ZrO_2-CeO_2-Dy_2O_3 at 1500°C and 1100°C has been developed. The solid solutions of limited solubility based on all components in their different polymorphic modifications were found and characterized. The fluorite (*Fm3m*) and cubic ($Ia\bar{3}$) and solid solutions are in equilibrium with all other phases existing in the system at these temperatures. The fluorite solid solution is represented by the largest homogeneity field originating from the sizes of F-fields in the two boundary binary systems CeO_2–Dy_2O_3 and ZrO_2–CeO_2 and ZrO_2–Dy_2O_3. The isothermal sections of the ZrO_2-CeO_2-Dy_2O_3 system at 1500°C contains two two-phase regions (F+C, T+F) and three two-phase regions (F+C, T+F, T+M) at 1100°C. With decreasing temperature from 1500°C down to 1100°C, the homogeneity regions on the basis of the cubic modification F-CeO_2(ZrO_2) narrow.

References:

1. He B., Zhao L., Wang W., Chen F., Xia C. (2011). Electro-catalytic activity of Dy_2O_3 as a solid oxide fuel cell anode material. *Electrochemistry Communications,* vol. 13, pp. 194–196.

2. Du W., Wang X., Li H., Ma D., Hou S., Zhang J., Qian X., Pang H. (2013). ZrO_2/Dy_2O_3 Solid Solution Nano-Materials: Tunable Composition, Visible light–Responsive Photocatalytic Activities and Reaction Mechanism. *Journal American Ceramic Society, v*ol. 96, no 9, pp. 2979–2986.

3. Kilner J. A. and Burriel M. (2014). Materials for Intermediate-Temperature Solid-Oxide Fuel Cells. *Annual Review of Materials Research*, vol. 44, pp 366–393.

4. Munawar A. U., Schulz U., Cerri G., Lau H. (2014). Microstructure and cyclic lifetime of Gd and Dy-containing EB-PVD TBCs deposited as single and double-layer on various bond coats. *Surface&Coatings Technology*, vol. 245, pp. 92–101.

5. Greshta V. (2015). Application of ceramic coatings for protection of GTE work in conditions of extremely high temperatures. *Vesnik dvyhatelestroenyya,* no 1, pp. 168–171.

6. Xu Q., Pan W., Wang J., Wan C., Qi L., Miao H. (2006). Rare-Earth Zirconate Ceramics with Fluorite Structure for Thermal Barrier Coatings. *Journal American Ceramics Society*, vol. 89, pp. 340–342.

7. Longo V., Roitti S. (1971). Solid State Phase Relations in the System CeO_2–ZrO_2, *Ceramurgia International*, vol. 1, no. 1, pp. 4–10.

8. Tani E., Yoshimura M., Somiya S. (1983). Revised Phase Diagram of the System ZrO_2–CeO_2 Bellow 1400°C, *Journal American Ceramics Society*, vol. 66, no 7, pp. 506–510.

9. Duran P., Gonzales M., Moure C., Jurado J. R., Pascual C. (1990). A New Tentative Phase Equilibrium Diagram for the ZrO_2–CeO_2 System in air. *Journal Material Sciety*, vol. 25, pp. 5001–5006.

10. Andrievskaya E.R., Red'ko V.P., Lopato L.M. (2001). Interaction of Cerium Oxide with Hafnia, Zirconia and Yttria at 1500°C, *Powder Metallurgia and Metal Ceramics*, vol. 40, no. 7–8, pp. 405–413.

11. Korniienko O.A. (2009). Interaction af properties of phases in the CeO_2 – Gd_2O_3 system at 1500°C [Interaction af properties of phases in the CeO_2 – Gd_2O_3 system at 1500°C]. *Visnyk NTU «KhPI»,* vol. 45, pp. 86–90.

12. Andrievskaya E.R, Kornienko O.A., Sameljuk A.V., Bykov A.I. Interaction of ceria and ytterbia in air within temperature range 1500–600° C. *Journal of the European Ceramic Society*, vol. 39, no. 9, pp. 2930–2935.

13. Andrievska E. R., Kornienko O. A., Sameliuk A. V., Sair A. (2020). Phase relation studies in the CeO_2-Eu_2O_3 system at 1500 to 600°C in air. *Journal Europium Ceramics Society*, vol. 40, pp. 751–758.

14. Andrievskaya E.R., Kornienko O.A., Sameljuk A.V., Sayir A. (2011). Phase Relation Studies in the CeO_2–La_2O_3 System at 1100–1500°C. *Journal Europia Ceramics Society*, vol. 31, no. 7, pp. 1277–1283.

15. Andrievskaya E.R., Kornienko O.A., Gorodov V.S. (2008). Phase relations in the CeO_2–Sm_2O_3 system at1500°C [Phase relations in the CeO_2–Sm_2O_3 system at 1500°C]. *Current problems of physical material science*, no. 17, pp. 25–29.

16. Grover V. and Tyagi A.K. (2008). Inter matrix fuels: materials for futuristic nuclear reactors. Founder's day. *Special Issue*, no. 297, pp. 160–164.

17. Grover V., Tyagi A.K. (2013). Ternary phase relations in CeO_2–$DyO_{1.5}$–ZrO_2 system. *Ceramics International*, vol. 39, pp. 7563–7569.

18. Kornienko O.A. (2014). Phase relations in the CeO_2–Dy_2O_3 system at1500°C [Phase relations in the CeO_2–Dy_2O_3 system at 1500°C]. *Current problems of physical material science*, no. 22, pp. 25–29.

19. Mikuśkiewicz M., Stopyra M., Moskal G. (2015). Synthesis and thermal characterization of dysprosium zirconate. *Solid State Phenomena*, vol. 223, pp. 54–61.

20. Pascual C., Duran P. (1980). Phase relations and ordering in the dysprosia-zirconia system. *Journal Materials Sciety*, vol. 15, pp. 1701–1708.

21. Rouanet A. (1971). Contribution a l'etude des systemes zirconia – oxydes des lanthanides au voisinage de la fusion: Memoire de these. *Rev. Intern. Hautes Temper. et Refract,* vol. 8, no. 2, pp. 161–180.

22. Thormber M.R., Bevan D.J.M. (1970). Summerville E. Mixed oxides of hte typy MO_2 (fluorite) – M_2O_3 very phase studies in the system ZrO_2-M_2O_3 (M=Sc, Yb, Er, Dy). *Journal Solid State Chemistry*, vol. 1, pp. 545–553.

23. Gavrish A.M., Alekseenko L.S., Tarasova L.A., Orekhova G.P. (1981). Structure and certain properties of solid solutions in ZrO_2-Dy_2O_3 (R=Sm, Dy) systems. *Neorganic Material*, vol. 17, pp. 2066–2070.

24. Wang C., Zinkevich M., Aldinger F. (2007). Experimental study and thermodynamic assessment of the ZrO_2 –$DyO_{1.5}$ system. *International Journal of Materials Research*, vol. 98, pp. 91–98.

25. Grover V., Tyagi A.K. (2013). Ternary phase relationsin CeO_2–$DyO_{1.5}$–ZrO_2 system Ceramics International, vol. 39, pp. 7563–7569.

26. Korniienko O.A., Andrievskaya E.R., Bogatyryova J.D., Korychev S.F. (2016). Phase equilibria in the ZrO_2–Dy_2O_3 system at 1100 to 1500°C. *Kharkiv University Bulletin, Series «Chemical»,* vol. 27, no. 50, pp. 39–48.

27. Andrievskaya E.R., Kornienko O.A., Korychev S.F., Bogatyryova J.D. (2016). Phase equilibria in the ZrO_2-Dy_2O_3 system at 1100°C [Phase equilibria in the ZrO_2-Dy_2O_3 system at 1100°C]. *Odesa National University Herald. Chemistry,* vol. 21, no. 3, pp. 77–86.

28. Andrievskaya E.R. (2013). Phase equilibria in the systems of hafnia, zirconia, yttria with rare-earth oxides [Phase equilibria in the systems of hafnia, zirconia, yttria with rare-earth oxides]. Kiev: Naukova dumka, 472 p. (in Russian)